Efficiency-enhanced picosecond mid-infrared optical parametric downconversion based on a cascaded optical superlattice

Shifeng Li (李世凤)[1], Panpan Ju (居盼盼)[1], Yanhua Liu (刘艳花)[2], Xudong Jiang (蒋旭东)[1], Rui Ni (倪 睿)[1], Gang Zhao (赵 刚)[1], Xinjie Lv (吕新杰)[1,*], and Shining Zhu (祝世宁)[1]

[1]*National Laboratory of Solid State Microstructures, Nanjing University, Nanjing 210093, China*

[2]*College of Physics, Optoelectronics and Energy & Collaborative Innovation Center of Suzhou Nano Science and Technology, Soochow University, Suzhou 215006, China*

**Corresponding author: lvxinjie@nju.edu.cn*

Received December 28, 2015; accepted March 4, 2016; posted online April 1, 2016

We demonstrate an efficiency-enhanced picosecond (ps) mid-infrared radiation via optical parametric downconversion. Based on a cascaded periodically poled MgO-doped stoichiometric lithium tantalate crystal (MgO:sPPLT), a tandem optical parametric oscillation-optical parametric amplification (OPO-OPA) process is achieved. Compared with a single OPO process, the conversion efficiency obtains an enhancement of 71%.

OCIS codes: 140.0140, 190.0190.
doi: 10.3788/COL201614.041402.

Ultrafast laser radiation with picosecond (ps) duration in the 2–5 μm mid-infrared region plays a key role in many fields including material processing, time-domain spectroscopy, countermeasures, and biomedical applications[1–3]. The synchronously pumped optical parametric oscillation (OPO) combined with the quasi-phase-matching (QPM) technique is a versatile means of generating tunable mid-infrared ps laser pulses. Crystals including periodically poled lithium tantalite (PPLT) and periodically poled lithium niobate (PPLN) are widely used in these OPOs[4–8]. However, according to the Manley–Rowe relation[9], when the idler wavelength increases the pump-to-idler efficiency decreases. For example, under the condition of $\lambda_p = 1$ μm and 100% quantum efficiency, if the idler wavelength is 2 μm, the conversion efficiency is 50%, whereas if the idler wavelength is 4 μm, the conversion efficiency is limited to 25%. On the other hand, the transmission of the light above 3.8 μm also decreases with the increase of the wavelength[10], another factor restricting the conversion efficiency from the pump to the idler in the longer idler wavelength region.

To increase the pump-to-idler efficiency, some approaches have been employed in previous studies, including optimizing the pump source[6] and the output coupling of the OPO[7]. The conversion efficiency can also be improved by extracting the residual energy from the signal light. For example, in 2000, McEwan and Terry demonstrated a tandem synchronously pumped OPO (SPOPO) employing two PPLN crystals within a cavity in which the second crystal in the OPO device converted the signal beam produced in the first crystal[11]. Then, Guo *et al.* proposed a difference frequency generation cascaded OPO based theoretically on a single superlattice that simplified the tandem nonlinear conversion system[12]. Based on this theory, our group designed and fabricated a dual-periodic superlattice and a tandem one, respectively, both achieving an optical parametric amplification (OPA)-assisted-OPO process operating in the nanosecond (ns) region, in 2011[13] and 2012[14]. In this Letter, we extended this scheme to the ps region, obtaining an efficiency-enhanced mid-infrared ps radiation at 3.87 μm, a wavelength noted for its military applications.

MgO:SLT was chosen as the nonlinear crystal for its large damage threshold[15], which is preferable in situations with high power. The cascaded process can be expressed as

$$\text{OPO: } \lambda_P \rightarrow \lambda_{s1} + \lambda_i \tag{1}$$

$$\text{OPA: } \lambda_{s1} \rightarrow \lambda_{s2} + \lambda_i, \tag{2}$$

where λ_P, λ_s, and λ_i represent the wavelength of the pump, signal and idler, respectively. The signal light generated from the first process acts as the pump light in the second process to further amplify the idler light. The two sections of the crystal were designed on the basis of the momentum conservation condition,

$$\Delta k_{\text{OPO}} = k_p - k_{s1} - k_i - G_{\text{OPO}} = 0, \tag{3}$$

$$\Delta k_{\text{OPA}} = k_{s1} - k_{s2} - k_i - G_{\text{OPA}} = 0, \tag{4}$$

where $G_{\text{OPO}} = \frac{2\pi}{\Lambda_{\text{OPO}}}$ and $G_{\text{OPA}} = \frac{2\pi}{\Lambda_{\text{OPA}}}$ are the reciprocal vectors of the two sections of the crystal and Λ_{OPO} and Λ_{OPA} are the poling periods of the two sections. According to the Sellmeier equation of MgO:SLT[16], we designed two tandem poling periods of 28.83 and 31.59 μm, respectively, to compensate for the phase mismatch of the following OPO and OPA process:

$$\text{OPO: } 1.064\ \mu\text{m} \rightarrow 1.47\ \mu\text{m} + 3.87\ \mu\text{m}, \tag{5}$$

$$\text{OPA: } 1.47\ \mu\text{m} \rightarrow 3.87\ \mu\text{m} + 2.37\ \mu\text{m}. \tag{6}$$

Taking the plane wave and the slowly varying envelope approximations, the parametric interaction between the amplitudes can be described by the coupling equations, under the perfect phase matching condition[11]:

$$\begin{aligned}
\frac{dA_p(z)}{dz} &= i\kappa_{\text{OPO}} A_{s1}(z) A_i(z),\\
\frac{dA_{s1}(z)}{dz} &= i\kappa_{\text{OPO}} A_p(z) A_i^*(z) + i\kappa_{\text{OPA}} A_i(z) A_{s2}(z),\\
\frac{dA_i(z)}{dz} &= i\kappa_{\text{OPO}} A_p(z) A_{s1}^*(z) + i\kappa_{\text{OPA}} A_s(z) A_{s2}^*(z),\\
\frac{dA_{s2}(z)}{dz} &= i\kappa_{\text{OPA}} A_{s1}(z) A_i^*(z).
\end{aligned} \tag{7}$$

In the above equations, $\kappa_{\text{OPO}} = \frac{d_{\text{eff}}}{c}\sqrt{\frac{\omega_p \omega_{s1} \omega_i}{n_p n_{s1} n_i}}$ and $\kappa_{\text{OPA}} = \frac{d_{\text{eff}}}{c}\sqrt{\frac{\omega_{s1} \omega_{s2} \omega_i}{n_{s1} n_{s2} n_i}}$ are coupling coefficients, where $d_{\text{eff}} = \frac{2}{\pi} d_{33}$ is the second-order nonlinear effective coefficient; c is the vacuum light velocity; and A_j, n_j are the amplitudes and refractive indices of ω_j $(j = p, s, s_2, i,)$, respectively.

Figure 1 shows the schematic diagram of the crystal structure. The OPO section is a bit wider than the OPA section, hence the single OPO process can be measured independently. The lengths of the two sections are 24 and 19 mm, respectively. The two end faces of the crystal are polished and coated as follows: HT@1064 nm (T > 95%), HT@1400–1500 nm (T > 99%), HT@3800–4200 nm (T > 90%). The crystal is housed in a self-fabricated oven with an accuracy of 0.1°C. In the first stage of the cascaded process, the pump λ_P is downconverted to λ_{s1} and λ_{i1}. Then, in the second stage, λ_{s1} acting as pump is downconverted to λ_{s2} and λ_{i2}. Only when $\lambda_{i1} = \lambda_{i2}$, the cascaded OPO-OPA process occurs and λ_{i1} generated in the first stage can be further amplified in the second stage. According to Fig. 1 in Ref. [11], the theoretical phase matching for the OPO-OPA process occurs at t = 145°C, which is the crossover point for the OPO and OPA curves. But in our experiment, the phase-matching temperature was measured to be approximately 110°C. The difference between theoretical and experimental phase-matching temperature is due to the inaccuracies of the Sellmeier equation and the thermal expansion of the crystal.

The experimental configuration is shown in Fig. 2. The pump source is a passively mode-locked ps Nd:YVO_4 laser,

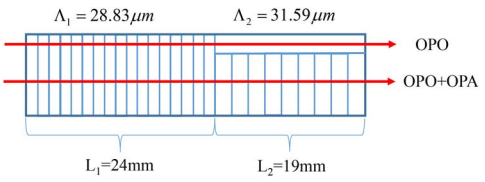

Fig. 1. Schematic diagram of the crystal structure.

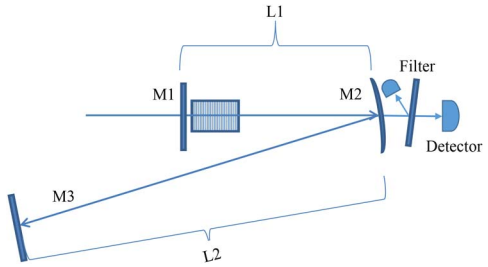

Fig. 2. Schematic configuration of the experimental setup.

delivering up to 20 W@1064 nm, linearly polarized, TEM_{00} mode, with a pulse duration of 28 ps and a repetition rate of 80 MHz. The OPO resonator is configured in a V cavity that is formed by one concave mirror with a radius of −500 mm and two plane mirrors. Both M_1 and M_2 are anti-reflection coated for 1064 and 3800–4200 nm, and high-reflection coated for 1400–1500 nm. M_3 is anti-reflection coated for 1064 nm, high-reflection coated for 1400–1500 nm, and also anti-reflection coated for 1650 nm to avoid unwanted resonances. The total optical length between M_1 and M_3 is 1.875 m to realize synchronous pumping. The beam waist of the cavity mode is calculated to be about 100 μm and is focused onto the crystal. In order to achieve perfect synchronous pumping, the cavity length should be adjusted accurately, which was realized by precisely changing the position of M_3.

The idler light power was measured after M_2. First, we characterized the single OPO process. As shown in Fig. 3, the maximum output power of 1.3 W was obtained at the pump power of 17.2 W, with a conversion efficiency of 7.6%, and the slope efficiency was calculated to be 8%. Subsequently, we moved the transverse position of the crystal to study the cascaded OPO-OPA process. Figure 4 shows the normalized idler power as a function of temperature. As can be seen from the figure, the maximum idler power was obtained at t = 110°C, which meant that the

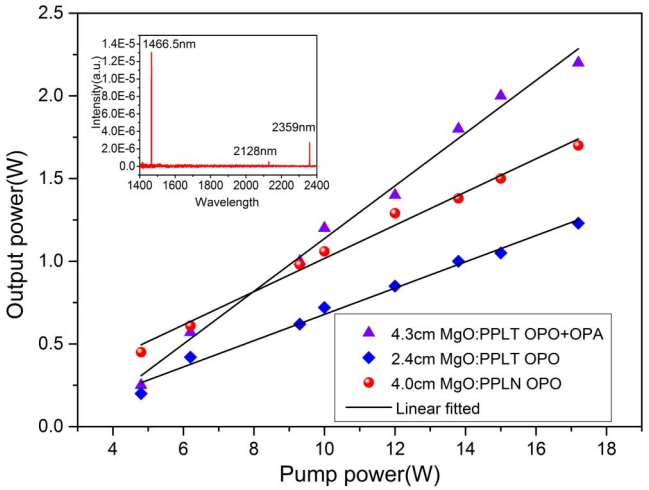

Fig. 3. Measured mid-infrared output of the single OPO and OPO-OPA versus pump power at 110°C. Insert is the output spectrum.

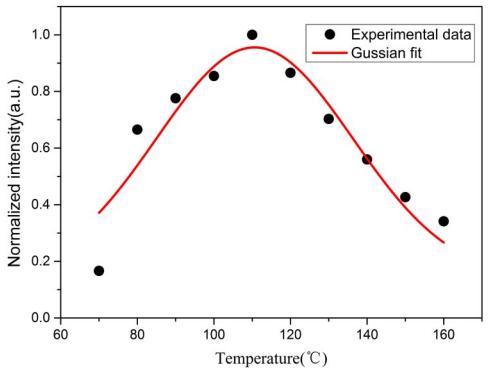

Fig. 4. Normalized intensity of the idler output power as a function of temperature.

cascaded OPO-OPA process occurred at this temperature. Gauss fitting results shows the temperature bandwidth is approximately 60°C. The spectrum captured by a spectra analyzer (YOKOGAWA AQ6375) at the temperature of 110°C is inserted in Fig. 3. The peaks, 1466.5 and 2359 nm, are at the wavelengths of λ_{s1} and λ_{s2}, respectively. From the measured spectrum, λ_i is calculated to be 3876 nm. Consequently, the actual OPO-OPA process in our experiment is:

$$\text{OPO: } 1064\ \text{nm} \rightarrow 1466.5\ \text{nm} + 3876\ \text{nm}, \quad (8)$$

$$\text{OPA: } 1466.5\ \text{nm} \rightarrow 2359\ \text{nm} + 3876\ \text{nm}, \quad (9)$$

which is in good agreement with the experimental design.

The output power of the cascaded OPO-OPA process at different pump conditions was also measured and is shown in Fig. 3. As can be seen from Fig. 3, the maximum output power reaches as high as 2.2 W, with a corresponding conversion efficiency of 13%. The slope efficiency is calculated to be 15.9%. Compared with the single OPO process, the maximum output power of the cascaded process increases by 69.2% and the conversion efficiency increases by 71%.

In addition, we also studied the output power of a single OPO process based on a 4 cm-long MgO:PPLN with a grating period of 28.7 μm. The measurement was carried out at t = 180°C, hence the wavelength of the output idler light was in accordance with the cascaded OPO-OPA process. The results are also shown in Fig. 3. As can be seen from the figure, the maximum idler power is 1.75 W, with a conversion efficiency of 10.2%, and the slope efficiency is 10%. Though the effective coefficient of MgO:PPLN is almost twice that of MgO:PPLT, and the length of the two crystals are almost the same, the pump-to-idler conversion efficiency of 4 cm-long MgO:PPLN is lower than that of the cascaded MgO:PPLT.

In the OPO process, the efficiency from the pump to idler is limited to λ_p/λ_i. However, in the cascaded OPO-OPA process, under the assumption that all of the signal light λ_{s1} generated from the first process can be converted to λ_{s2} and λ_i in the second OPA process, the total conversion efficiency limitation is $2\lambda_p/\lambda_i$.

In conclusion, we demonstrate a cascaded ps OPO-OPA process based on a tandem MgO:sPPLT chip. Compared with a single OPO process, both the maximum output power of mid-infrared idler light and the corresponding conversion efficiency increase dramatically. By optimizing the experimental configuration and increasing the pump power, we can expect a much higher output power.

This work was supported by the International Science and Technology Cooperation Program of China (ISTCP) (No. 2014DFT50230), the National Key Scientific Instrument and Equipment Development Project (No. 2011YQ030127), and the National Natural Science Foundation of China (No. 61405133).

References

1. C. W. Freudiger, W. Min, B. G. Saar, S. Lu, G. R. Holtom, C. W. He, J. C. Tsai, J. X. Kang, and X. S. Xie, Science **322**, 1857 (2008).
2. M. Jurna, J. P. Korterik, and H. L. Offerhaus, Appl. Phys. Lett. **89**, 251116 (2006).
3. W. Dai, Y. Song, B. Xu, A. Martinez, S. Yamashita, M. Hu, and C. Wang, Chin. Opt. Lett. **12**, 111402 (2014).
4. O. Kokabee, A. Esteban-Martin, and M. Ebrahim-Zadeh, Opt. Lett. **35**, 3210 (2010).
5. G. Zhao, P. P. Ju, X. J. Lu, Z. H. Shi, Y. T. Huang, and X. Y. Liang, Acta Sin. Quant. Opt. **20**, 172 (2014).
6. K. Z. Han, J. Ning, J. L. He, J. Hou, B. T. Zhang, and Z. W. Wang, Chin. Phys. Lett. **32**, 054203 (2015).
7. S. C. Kumar and M. Ebrahim-Zadeh, Opt. Express **19**, 26660 (2011).
8. W. Tian, J. Zhu, Z. Wang, and Z. Wei, Chin. Opt. Lett. **13**, 011901 (2015).
9. J. M. Fraser and C. Ventalon, Appl. Opt. **45**, 4109 (2006).
10. A. Smith, http://www.as-photonics.com/snlo.
11. K. J. McEwan and J. A. C. Terry, Opt. Commun. **182**, 423 (2000).
12. H. C. Guo, Y. Q. Qin, Z. X. Shen, and S. H. Tang, J. Phys. Condens. Matter **16**, 8465 (2004).
13. Y. H. Liu, Z. D. Xie, W. Ling, Y. Yuan, X. J. Lv, J. Lu, X. P. Hu, G. Zhao, and S.N. Zhu, Opt. Express **19**, 17500 (2011).
14. Y. H. Liu, X. J. Lv, Z. D. Xie, X.P. Hu, Y. Yuan, J. Lu, L.N. Zhao, G. Zhao, and S.N. Zhu, Appl. Phys. B **106**, 267 (2012).
15. X. P. Hu, X. Wang, J. L. He, Y. X. Fan, S. N. Zhu, H. T. Wang, Y. Y. Zhu, and N. B. Ming, Appl. Phys. Lett. **85**, 188 (2004).
16. W. L. Weng, Y. W. Liu, and X. Q. Zhang, Chin. Phys. Lett. **25**, 4303 (2008).